

Development of a stress-induced martensitic transformation criterion for a Cu–Al–Be polycrystalline shape memory alloy undergoing uniaxial tension



F.N. García-Castillo^{a,*}, J. Cortés-Pérez^b, V. Amigó^c, F.M. Sánchez-Arévalo^d, G.A. Lara-Rodríguez^d

^a Posgrado de Ingeniería, Facultad de Ingeniería, Universidad Nacional Autónoma de México, Circuito Exterior, Ciudad Universitaria, México, D.F. C.P. 04510, Mexico

^b Centro Tecnológico Aragón, FES Aragón, UNAM. Av. Rancho Seco s/n, Col. Impulsora, Cd. Nezahualcóyotl, Estado de México, C.P. 57130, Mexico

^c Universitat Politècnica de València, Instituto de Tecnología de Materiales, Camino de Vera s/n, C.P. 46022, Spain

^d Instituto de Investigaciones en Materiales, Universidad Nacional Autónoma de México, Apdo. Postal 70-360, Cd. Universitaria, México, D.F. C.P. 04510, Mexico

ARTICLE INFO

Article history:

Received 12 February 2015

Revised 17 June 2015

Accepted 21 June 2015

Available online 12 July 2015

Keywords:

Shape memory materials

Grain interaction

Stress-induced martensitic transformation

EBSD

ABSTRACT

This study presents a criterion for predicting the martensitic variants (MVs) that appear during the stress-induced martensitic transformation (SIMT) in a polycrystalline sample of Cu–11.5% wt. Al–0.5% wt. Be under simple tension. Our criterion is based on crystallographic parameters, such as the crystal orientation and Schmid factor (*SF*). The displacement vector fields (*DVFs*) were obtained in the observation system by a mathematical model and were used to distort the boundary of a set of grains. From the *DVF*, the strain tensor for each grain was obtained, and the strain ratio (*SR*) in the observation system was calculated. Electron backscattering diffraction (*EBS*) measurements were performed to determine the crystal orientation of the grains. The inverse *SF* was used to determine the in-plane stress transformation diagrams (*STDs*) for each studied grain. The combination of a balance criterion (*BC*) and *STD* provided a criterion that allowed us to predict the possible order of stress-induced MVs formed as a function of the crystal orientation and thermomechanical parameters of the shape memory alloy (*SMA*) with higher accuracy than when using the criteria separately. To validate our criteria, we tested other researchers' published results. Our results were in agreement and were capable of predicting the stress-induced MVs in a polycrystalline *SMA*.

© 2015 Acta Materialia Inc. Published by Elsevier Ltd. All rights reserved.

1. Introduction

In mechanical engineering applications, shape memory alloys (*SMA*s) are considered interesting materials due to their well-known effects. Such applications are focused on the development of sensor/actuator devices, which were recently applied to energy recovery [1–6]. Some of these applications would be quite complicated if conventional materials were used. The creation of new devices with *SMA*s requires the use of mathematical models that consider the associated effects of these materials and mimic their mechanical behavior appropriately.

Research conducted on these alloys indicates that their mechanical behavior is complex because of their highly anisotropic nature, non-linear mechanical behavior, hysteresis, and temperature dependence [7–11]. For these reasons, previous studies

have focused on single crystals [12–17]. However, the vast majority of applications require polycrystalline materials; therefore, some research has been conducted to understand the mechanical behavior of *SMA* polycrystals, and mathematical models and experimental results have been reported [18–20]. In fact, the relation between microstructure and macromechanical behavior has posed an interesting research problem for many years. The mechanical behavior of *SMA*s composed of polycrystalline materials is strongly altered by effects associated with their microstructure. For this reason, studies related to the stress-induced martensitic transformation (*SIMT*) of polycrystalline *SMA*s have taken into account specific issues such as the Hall–Petch relationship, grain interaction (*GI*) and the Schmid factor (*SF*) [21–28]. For example, according to Montecinos et al. [21], the change in the mechanical behavior of Cu–Al–Be under stress depends on its grain size. These results indicate a Hall–Petch-type relationship; however, the authors did not consider the crystallographic orientation and the martensitic variants (*MVs*) formed in each grain. Berveiller et al. [22] performed an in situ study of the lattice rotation of an individual grain during the *SIMT* of Cu–Al–Be samples

* Corresponding author.

E-mail addresses: fer_nes@hotmail.com (F.N. García-Castillo), jacop@unam.mx (J. Cortés-Pérez), vamigo@mcm.upv.es (V. Amigó), fsanchez@iim.unam.mx (F.M. Sánchez-Arévalo), laragab@iim.unam.mx (G.A. Lara-Rodríguez).

subjected to a tensile load at room temperature. These authors observed small changes in the crystal orientation after the inverse *SIMT*. Siredey et al. [23] developed a thermomechanical model that considers the interaction between the *MVs* of a grain and obtained an equation to mimic the interaction energy for more than two Cu–Al–Be *MVs*. Sánchez-Arévalo et al. [24] used a digital image correlation technique to obtain the displacement vector fields (*DVFs*) in a Cu–Al 11.2 wt.%–Be 0.6 wt.% *SMA* during the *SIMT* in a simple tensile test. Martínez-Fuentes et al. [25] applied the methodology developed by Sánchez-Arévalo et al. to observe the micromechanical and macromechanical behavior of a Cu–Al 11.2 wt.%–Be 0.6 wt.% polycrystal and a Cu–Al 11.2 wt.%–Be 0.5 wt.% single crystal *SMA* undergoing a *SIMT* induced by 3-point bending. These authors observed *GI* in the 2D confined grains, possibly because the interaction between the growing *MV* modified the local state of stress in the grain and neighboring grains. The martensitic phase re-orientates with increasing load, which provokes the growth of several *MVs* in different directions; this finding was in good agreement with the stress transformation diagrams (*STDs*) for Cu–Al–Be alloys. However, this study did not consider the crystallographic aspect of each grain studied.

The *SIMT* in *SMA*s provides a good opportunity to compare plasticity criteria to obtain other essential aspects of *SMA*s, such as the *SF*. Recently, some researchers have used the *SF* to study the *SIMT* in polycrystalline samples [26–28]. For example, Kaouache et al. [27] used this factor to verify the formation of *MVs* in polycrystalline samples during the *SIMT*, expanding the application of the *SF* criterion, which is typically used in single crystals, to polycrystalline samples.

In addition, mathematical models have been developed to mimic the macromechanical and micromechanical behavior of *SMA*s; specifically, we focus on the model of Cortés-Pérez [29]. This model is used to simulate the distortion of the sample surface and obtain the strain and displacement fields of an *SMA* undergoing the *SIMT* as a function of the crystalline orientation. The Cortés-Pérez model [29] consists of a mathematical description of the *DVF* present in a sample during the *SIMT*. This *DVF* is non-homogeneous and is defined in a reference system matching the transformation system (X_T, Y_T, Z_T) , where the unit base in the system is (e_{T1}, e_{T2}, e_{T3}) , as shown in Fig. 1. The other two systems used in this research appear in this figure as (X, Y, Z) and (X_0, Y_0, Z_0) with unit bases (e_1, e_2, e_3) and (e_{01}, e_{02}, e_{03}) , respectively.

The *DVF* $u(x_T, y_T, z_T)$ is defined for each transformation element (24 *MVs*); this vector field can be expressed by a habit plane $(n_1 \ n_2 \ n_3)$ and a shear direction $[m_1 \ m_2 \ m_3]$ with coordinates (x_T, y_T, z_T) . This *DVF* can be written as follows:

$$u(x_T, y_T, z_T) = \begin{pmatrix} \delta f h w(y_T) \\ 0 \\ 0 \end{pmatrix} \quad (1a)$$

$$w(y_T) = \begin{cases} 0; & -\infty \leq y_T \leq 0 \\ \frac{y_T}{hf}; & 0 \leq y_T \leq hf \\ 1; & hf \leq y_T \leq h \end{cases} \quad (1b)$$

where δ is the shear amplitude value and h is the length of the martensitic plate along the y_T direction.

Thus, $w(y_T)$ is re-defined using a smoothing double hyperbole:

$$w(y_T) = \frac{fh + \sqrt{r_0^2 + y_T^2} - \sqrt{r_0^2 + (y_T - fh)^2}}{2fh} \quad (2)$$

where r_0 is the radius of the transition of the martensitic–austenite boundaries and f is the volumetric fraction, a scalar value depending on the applied stress, test-temperature, and *SMA* parameters. The volumetric fraction is defined by Eq. (3),

$$f = \frac{e^{\frac{\ln(9)(2\sigma - \sigma_c - \sigma_f)}{\sigma_f - \sigma_c}}}{1 + e^{\frac{\ln(9)(2\sigma - \sigma_c - \sigma_f)}{\sigma_f - \sigma_c}}} \quad (3)$$

where σ is the applied effective stress (for the simple tension test, the applied effective stress is defined by the ratio of shear stress/*SF*, τ/m). σ_c and σ_f are the effective critical stresses at the beginning and end of the *SIMT*, respectively, at test temperature T ; these stresses can be calculated by the following equations, which consider the Clausius–Clapeyron ratio:

$$\sigma_c = \frac{\partial \sigma_c}{\partial M_s} (T - M_s) \quad (4)$$

$$\sigma_f = \frac{\partial \sigma_c}{\partial M_s} (T - M_f) \quad (5)$$

where M_s and M_f are the critical temperatures at the beginning and end of the martensitic transformation, respectively, which depend on the chemical composition and grain size, among other factors. The *DVF* is defined in the observation system and denoted as

$$(x_T, y_T, z_T)^T = A_{X_0 \rightarrow X_T} (x_0, y_0, z_0)^T \quad (6)$$

$$\begin{aligned} u(x_0, y_0, z_0) &= A_{X_T \rightarrow X_0} u(x_T, y_T, z_T) \\ &= A_{X_T \rightarrow X_0} u \left(\left(A_{X_0 \rightarrow X_T} (x_0, y_0, z_0)^T \right)^T \right) \end{aligned} \quad (7)$$

where the relation of the three-vector space basis used in this research is

$$A_{X_T \rightarrow X_0} = A_{X \rightarrow X_0} A_{X_T \rightarrow X} \quad (8)$$

The $A_{X_T \rightarrow X_0}$ matrix is used to change the basis from the transformation to observation system as a function of grain orientation and is defined as

$$A_{X \rightarrow X_T} = [A_{X_T \rightarrow X}]^{-1} = \sum_{i=1}^3 \{e_i\}_{X_T} \otimes e_i \quad (9)$$

$$A_{X_T \rightarrow X} = \sum_{i=1}^3 \{e_{T_i}\}_X \otimes e_{T_i} = \begin{pmatrix} m_1 & p_1 & n_1 \\ m_2 & p_2 & n_2 \\ m_3 & p_3 & n_3 \end{pmatrix} \quad (10)$$

$$A_{X \rightarrow X_0} = [A_{X_0 \rightarrow X}]^{-1} = \sum_{i=1}^3 \{e_i\}_{X_0} \otimes e_i \quad (11)$$

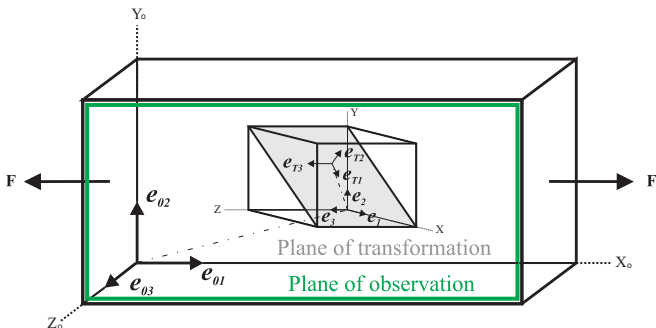


Fig. 1. Vector space basis used in the Cortés-Pérez model [29]: transformation basis e_{Ti} , observation basis e_{0i} , and “Canonic” basis e_i , $i = 1, 2, 3$.

$$A_{x_0 \rightarrow x} = \sum_{i=1}^3 \{e_{0i}\}_x \otimes e_{0i} = \begin{pmatrix} u & c_1 & h \\ v & c_2 & k \\ w & c_3 & l \end{pmatrix} \quad (12)$$

where $[h \ k \ l]$ is the sample normal (SN) and $[u \ v \ w]$ is the rolling direction (RD); the coordinates of the RD, (x_0, y_0, z_0) , are obtained from electron backscattering diffraction (EBSD); $(n_1 \ n_2 \ n_3)$ is the habit plane; and $[m_1 \ m_2 \ m_3]$ is the direction of the strain shear. Its coordinates are (x_T, y_T, z_T) . Both of these arrays are described by the canonic vector space basis, which is defined by the unit cell of the austenite phase. These transformation systems are different for each SMA. In addition, the transversal direction (TD) can be determined by the cross product of the SN and RD. Similarly, the third direction in the transformation system is determined by the cross product of the habit plane and the direction of deformation in each base:

$$\begin{pmatrix} p_1 \\ p_2 \\ p_3 \end{pmatrix} = \begin{pmatrix} m_1 \\ m_2 \\ m_3 \end{pmatrix} \times \begin{pmatrix} n_1 \\ n_2 \\ n_3 \end{pmatrix} \quad (13)$$

$$\begin{pmatrix} c_1 \\ c_2 \\ c_3 \end{pmatrix} = \begin{pmatrix} u \\ v \\ w \end{pmatrix} \times \begin{pmatrix} h \\ k \\ l \end{pmatrix} \quad (14)$$

Finally, the strain tensor is defined as the symmetric part of the displacement field gradient:

$$\varepsilon_{Tr} = \frac{1}{2} [\text{grad}(u(x_0, y_0, z_0)) + \text{grad}^T(u(x_0, y_0, z_0))] \quad (15)$$

The literature contains detailed accounts of extensive efforts to understand the nature of the SIMT; some of which have considered the crystal orientation and SMA parameters [27,28].

However, research on the SIMT has yet to enable a prediction of the possible order of MV formation as a function of crystallographic and SMA parameters; therefore, the aim of our study is to develop a novel criterion that theoretically predicts the formation of MVs on the observation surface for a set of grains by considering the crystal orientation and the parameters of the SMA, including the critical temperatures, the Clausius–Clapeyron relationship, and the transformation system.

Our research considers 10 grains of two different polycrystalline samples of a Cu–11.5 wt.% Al–0.5 wt.% Be SMA. The first sample was elaborated in this research, and the second involves a sample tested by Kaouache et al. [27]; their results are considered in our study. The crystallographic orientation of each grain in our sample was measured using the EBSD technique. Hence, the 24 MVs were depicted in the observation system for all the studied grains and were compared with the MVs obtained during the SIMT. The strain ratio (SR) criterion was used to predict the MVs. The strain tensor was determined using the DVF obtained from the Cortés–Pérez model [29]. The DVF in the system of observation was used to distort the grain perimeter (obtained by digital image analysis of each studied grain). Next, a set of three grains with a common triple point was compared before and after the transformation. Because the |SR| and SF criteria were not sufficient to allow a prediction of the MVs, an additional criterion was introduced, which considers the balance between both the |SR| and the SF criteria to predict the order of formation of the MVs. This criterion is complemented with the in-plane STDs.

2. Experimental details

A polycrystalline sample of Cu–11.5 wt. Al–0.5 wt. Be was produced by conventional casting techniques in a high-frequency furnace. This alloy was elaborated using Belkahl's equation [30].

An ingot was obtained from this cast. Then, thin slides were cut to $18 \times 10 \times 1.2$ mm ($l \times w \times t$) using an Accutomm-5 automatic precision cut-off machine from Struers Izasa S.A. (Barcelona, Spain). A recirculation-cooling unit with a flow rate of 800 ml/min and a constant speed of 0.025 mm/s was used.

From the thin slides, one sample was obtained with a reduced-center section of 4 mm. After sample preparation, the samples were betatized (750 °C for 15 min and 100 °C for 20 min) according to the method of Flores [31]. Then, the M_5 temperature was determined using a TA Instruments Q100 differential scanning calorimeter (DSC) (New Castle, Delaware, United States) with a 39.45 mg sample. DSC was performed over a temperature range from –80 to 200 °C at a rate of 20 °C/min.

To observe the crystalline microstructure of these materials, the tensile samples were prepared for metallography according to the standards of Struers for Cu preparation; because of the size of the samples, only mechanical polishing was used under small applied loads, avoiding the SIMT. This metallographic preparation was adequate for EBSD measurements, which were performed to detect the crystalline orientation of the grains. The EBSD measurements were performed in a JEOL model JSM 6300 scanning electron microscope with INCA software. In this software, the crystallographic parameters of Cu–Al–Be must be input as follows: DO_3 bcc, $a_0 = 5.82$ Å and special group $Fm\bar{3}m$ (225) [32]. The uniaxial tensile tests were then conducted on a Deben–Gatan Microtest tensile device (Gatan, Inc., Pleasanton, California, United States), which was coupled to an optical microscope from Leica MZ APO. The equipment included a 2 kN load cell, and the deformation rate of these tests was 0.2 mm/min. The SIMT was also observed in situ. A specially programmed virtual instrument in LabView was used to detect grain boundaries, registering a set of (x, y) points, which defined the geometry of each grain. This analysis was conducted after the EBSD measurements because EBSD was able to reveal the grains without any chemical etching. A front panel of the grain-boundary detection virtual instrument is presented in Fig. 2.

The parameters used for the Cu–Al–Be sample in our calculations were $M_5 = -20$ °C, based on DSC measurements; a Clausius–Clapeyron relation of $d\sigma/dT = 1.97 \frac{\text{MPa}}{^\circ\text{C}}$ [33]; a shear amplitude of 0.2324; and the transformation system reported by Kajiwara et al. [34] for the Cu–Al system $n = [0.17, 0.66, 0.72]$ and $m = [0.16, -0.74, 0.64]$.

3. Results and discussion

Two separate regions were observed in our sample and are presented as regions R1 and R2 in Fig. 2a. Only 3 grains were analyzed in each region. The crystalline orientation of grains is required to apply our SIMT criterion. Fig. 3a and b present images of the microstructures in the austenite phase for regions R1 and R2 obtained from EBSD measurements; these figures provide the labels for the six grains analyzed in this study. The images are colored according to the crystal orientation depicted by the inverse pole figure, and the color key is provided in Fig. 3c; Fig. 3a and b were plotted on the RD. The EBSD measurements were obtained after the first cycle of uniaxial tension. The crystallographic details of these grains are summarized in Table 1.

Fig. 4 presents typical MVs formed by the SIMT of the studied grains; these plates are similar to those previously reported by other authors [23–28]. In this figure, our sample was at a specific stress higher than the critical stress of transformation, σ_c .

The grains contained in R1 (42, 43 and 63) indicate that the vast majority of the MVs had a similar angle on the e_{01} axis; however, this result does not imply that the same stress-induced MV has been obtained. To prove this case, the crystallographic orientation of each grain and the transformation system reported by Kajiwara

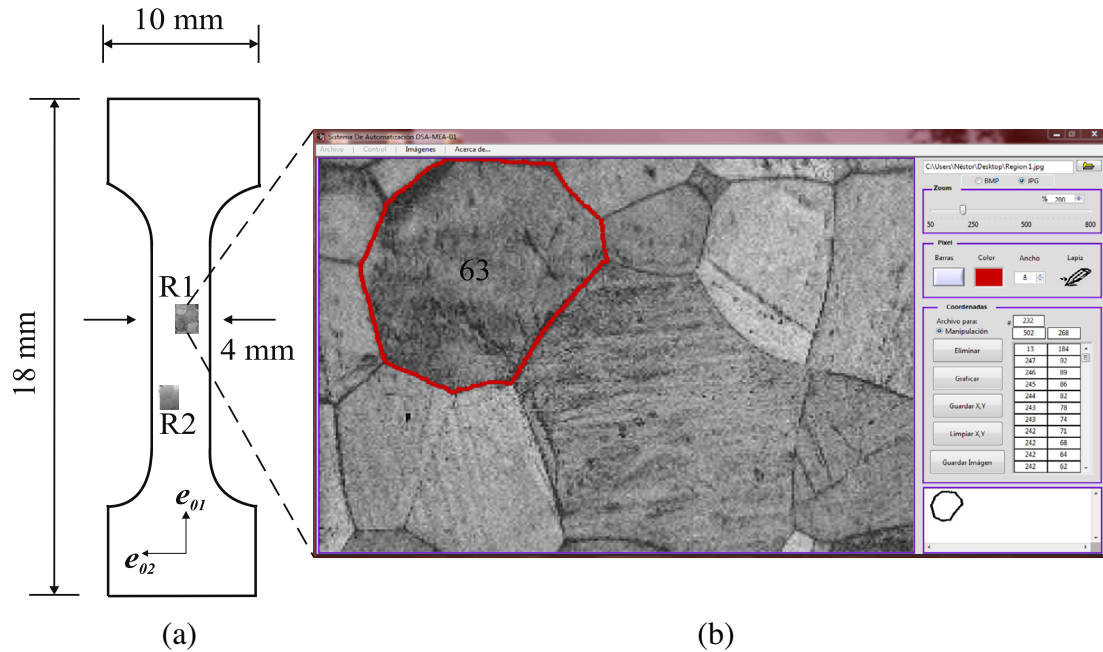


Fig. 2. Digital images used for the detection of a grain perimeter. (a) Tensile sample illustrating the dimensions and specific studied regions. (b) Front panel of the virtual instrument, which shows the window corresponding to the “routine” to select and record points on the boundaries of the grain.

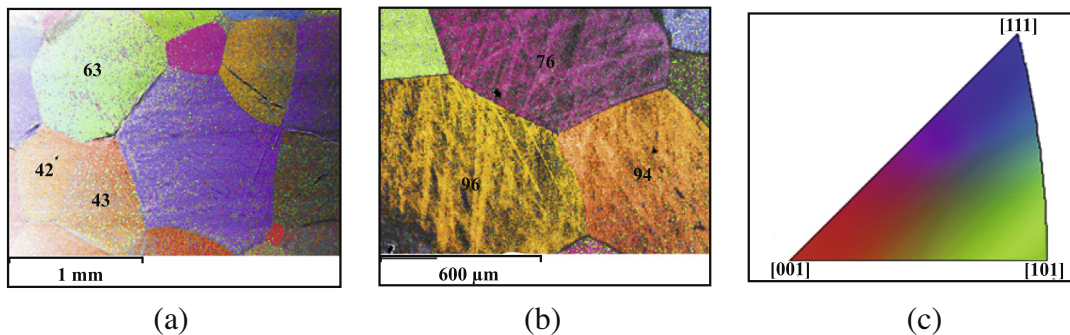


Fig. 3. Measurements of the EBSD for the Cu–Al–Be SMA. (a) Region 1 involving grains 42, 43, and 63. (b) Region 2 involving grains 76, 94, and 96. (c) Color key of the inverse pole figure.

Table 1
Crystallographic orientations of each grain studied in our sample.

Region 1			Region 2		
Grain	RD	SN	Grain	RD	SN
42	[0.19, 0.89, -0.39]	(0.10, -0.42, -0.89)	76	[-0.46, -0.85, -0.23]	(0.88, -0.41, -0.23)
43	[-0.42, 0.38, 0.81]	(0.10, 0.91, -0.37)	94	[0.88, -0.22, -0.41]	(0.40, -0.10, 0.90)
63	[0.15, 0.97, -0.15]	(0.78, -0.21, -0.57)	96	[0.86, 0.37, -0.34]	(0.39, -0.91, 0)

et al. [34] were used to obtain the 24 MVs for the observation system. The order of the transformation system in this research is the same as that reported by Kaouache et al. [27]. Each mark on the observation surface was calculated using the matrix for the change of basis applied to the corresponding habit plane; their intersection with the observational plane was subsequently obtained. This analysis was performed for the six grains studied in our sample; however, Fig. 5 only provides the diagram for grain 43.

The perimeter of grain 43 is denoted by a black dotted line, whereas the e_{01} and e_{02} axes (the RD and TD directions, respectively) are denoted by black dot-dashed lines, according to the

basis defined in Fig. 1. In relation to the color code of Fig. 5, the important obtained MVs are 3, 4, 11, and 12 (gray, dark gray, light brown and light orange, respectively). The calculations show that four MVs calculated are coincident, with only one MV formed at $107 \pm 1^\circ$ with respect to the e_{01} axis, as shown in Fig. 5b. Similarly, the intersection of each habit plane with the observational plane was calculated for each grain, and the results are summarized in Table 2.

In addition, the MVs coincident with the real MVs were filed according to the number of MVs formed in each grain. For example, 3 MVs were formed in grain 63; therefore, calculated MVs 23 and

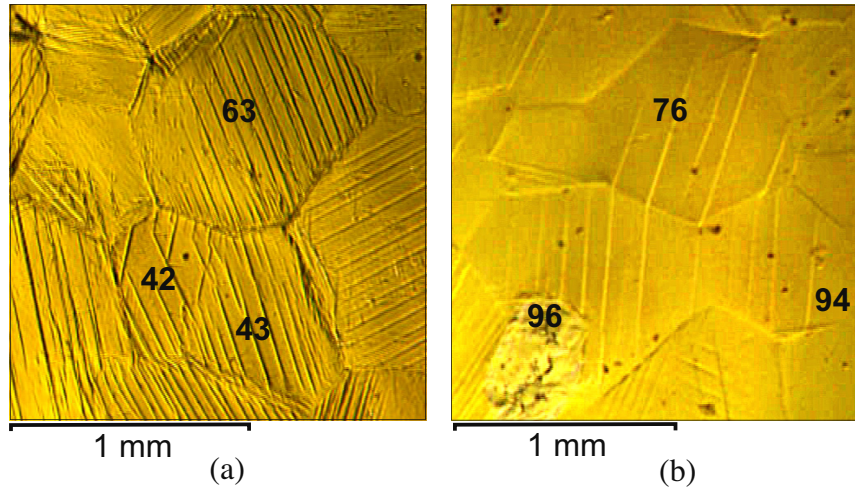
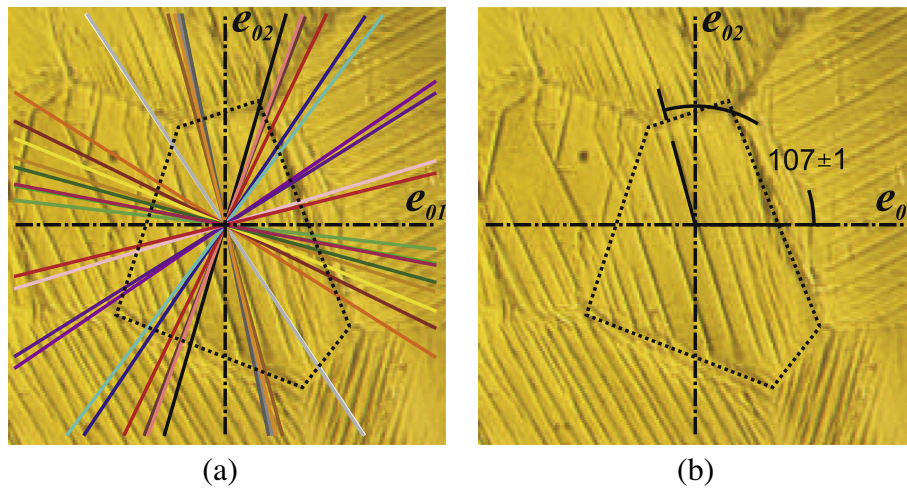


Fig. 4. Formed MVs of each grain studied in our sample. (a) Region 1. (b) Region 2.



Variant	1	2	3	4	5	6	7	8	9	10	11	12
Color	□	□	□	□	□	□	□	□	□	□	□	□
Variant	13	14	15	16	17	18	19	20	21	22	23	24
Color	□	□	□	□	□	□	□	□	□	□	□	□

Fig. 5. MVs formed and calculated in grain 43. (a) Diagram of the 24 possible MVs overlapped on the metallographic image. (b) Average angle formed between the e_{01} axis and the real MV.

24 are coincident with only one of the formed MVs. Finally, Table 2 provides the angle deviation between the calculated and real MVs formed for each case. The selected MVs were within an angle of less than 10° , which suggests misalignment in the studied samples.

Because several MVs may match the real MVs for the grains, it was necessary to establish a criterion to select the real MV that grows in the plane of observation.

One method of discarding some MVs is the SF criterion, as previously reported by Kaouache et al. [27]. Table 3 presents three expected MVs with the highest SF for each grain, and the last column provides the MVs that matched those in Table 2 for the six studied grains in regions R1 and R2.

Our experimental results and the SF criterion indicated that only grains 43 and 63 satisfied the condition of the maximum SF criterion. These results are inconsistent with the criteria reported by Kaouache et al. [27]. For this reason, we performed an analysis to compare our results with those reported by Kaouache et al. [27]. This analysis was the same as that used for our samples. The 24 MVs in the observation system were calculated for all grains

reported by Kaouache et al. [27]. The real MVs formed and the calculated MVs are compared in Table 4. The SF for the 24 MVs of each grain reported by Kaouache et al. [27] was recalculated. We used the following crystallographic orientations to obtain the same MVs reported by Kaouache et al. [27] for grain C–SN ($-0.84, -0.13, -0.52$) and RD [$0.27, -0.94, -0.16$]—according to the method of Cortés–Pérez et al. [35].

A comparison of the results from Tables 4 and 5 indicates that the MV with maximum SF is always present in the actual case, as described by Kaouache et al. [27]; nevertheless, the second MV, with a higher probability of growth, does not always satisfy this condition.

As previously discussed, our results indicate that the MV with the higher SF did not always grow. The third MV with a high SF (but not the highest) appeared in the plane of observation, as shown in Table 3 for grains 42, 43, 63, 76 and 94.

To explain why the third MV with a high SF value grows instead of the MV with maximum SF, we first calculated the strain tensor in the observation system and the SR ($\epsilon_{x0}/\epsilon_{y0}$) for the three expected

Table 2
Summary of the comparison between the formed and calculated MVs in our sample.

Region	Grain	MVs formed by grain	Calculated MVs	Angle deviation between calculated and formed MVs (°)		
1	42	I	2	2.9		
			3	6.1		
		II	4	6.4		
			9	5.8		
			10	8.9		
	43	I	3	1.4		
			4	1.9		
			11	2.8		
			12	0		
			23	0		
	63	I	24	2.4		
			9	3.9		
			10	0		
			11	8		
			18	9.5		
			19	0.9		
		II	20	5.7		
8			1.1			
17			6.6			
2			76	I	17	2.5
					18	6.5
					23	1.1
	24	1.9				
	94	I		5	3.7	
6			4.8			
15			6.2			
16			3.8			
96	I	17	2			
		18	0.5			

Table 3
Expected and coincident MVs, according to the SF criterion, of grains studied in R1 and R2.

Region	Grain	Expected MVs	Highest SF	Formed MVs
1	42	19	0.47	None
		24	0.42	None
		2	0.38	I
	43	11	0.36	I
		14	0.34	None
		3	0.29	I
	63	19	0.49	II
		2	0.49	None
		24	0.45	I
	2	76	12	0.44
2			0.39	None
17			0.33	I
94		23	0.45	None
		18	0.41	None
		15	0.37	I
96		13	0.41	None
		18	0.39	I
		8	0.33	None

MVs with high SFs using the model of Cortés–Pérez [29]. Fig. 6 illustrates the meaning of the SR. Specifically, this figure presents two patterns of distortion for grains from region 2. Both patterns of displacement were obtained in the mathematical model developed by Cortés–Pérez [29]. This model is able to simulate the displacement and deformation fields encountered by a grain during the growth of an MV.

Fig. 6a presents the initial configuration of the perimeters of grains 76, 94, and 96 (without deformation and before the martensitic transformation). Then, applying the model of Cortés–Pérez [29] for each individual grain, a deformed configuration is obtained and shown in Fig. 6b and c. This model also provides us with the

DVF for each MV in each grain for two cases. The first case corresponds to the DVF associated with MVs that presented a maximum SF (VMSF), in which case the DVF presents a large displacement component in the TD (e_{02}). The second case corresponds to the DVF associated with MVs that presented a higher SR (VHSR), in which case the DVFs were largely aligned with the e_{01} direction. Considering both types of distortion (VMSF and VHSR), a GI effect was clearly observed. The VMSF distortion demonstrated a tensile state of stress, causing a grain separation trend, whereas the VHSR exhibited the opposite trend, with lower-magnitude compression and tension states of stress relative to those observed for VMSF. Both types of distortion can contribute strongly to the stress in these grains. This contribution might alter the growth of the expected MVs or even inhibit the growth of an MV with a maximum SF; this latter condition is stronger for VHSR distortion. Importantly, strain compatibility is more likely to be preserved in VHSR than in VMSF. This tendency can be predicted by analyzing the strain tensor, namely, the proposed SR. Such an effect could be explained as a tendency for the material to employ the minimal mechanical energy, released during the tension test, to begin martensitic nucleation caused induced by stress. Finally, Fig. 6d presents the actual stress-induced MVs for grains 76, 94, and 96. The VHSR clearly corresponds well with the actual MVs presented in Fig. 6d.

Fig. 6 presents the analysis for three grains, although several additional grains were analyzed. The results of this analysis are summarized in Table 6. In this case, we compared the 24 MVs

Table 4
Summary of the comparison between the formed and calculated MVs for samples P1 and P2 reported by Kaouache et al. [27].

Sample	Grain	MVs formed by grain	Calculated MVs	Angle deviation between calculated and formed MVs (°)	
P1	A1	I	3	0	
			4	0	
			11	7.2	
			12	7.4	
			5	5.4	
		B1	I	6	0
				7	9.3
				8	2
				9	1.4
				10	4.9
	C1	II	13	7.3	
			15	3.7	
			16	0.7	
			12	3.5	
			14	2.7	
			21	7.1	
		III	I	22	1.2
				9	5.4
				10	1
				15	1.8
				24	6.5
				19	0
P2	A2	I	17	2.3	
			18	0	
			4	1.1	
			5	0.9	
			23	2.3	
	B2	II	6	4.7	
			3	5.8	
			7	7.6	
			8	3.9	
			24	3.9	

Table 5
Expected and coincident variants, according to the SF criterion, of grains reported by Kaouache et al. [27].

Sample	Grain	Expected MVs	Highest SF	Formed MVs
P1	A1	4	0.42	I
		10	0.38	None
		6	0.26	None
	B1	6	0.47	I
		15	0.47	II
		21	0.32	III
C1	10	0.49	I	
	4	0.45	None	
	22	0.45	III	
P2	A2	18	0.40	I
		23	0.39	II
		3	0.33	III

plotted for each grain and the MV with the highest absolute value of strain ratio ($|SR|$).

The same analysis was also applied to the grains reported by Kaouache et al. [27]; the results are summarized in Table 7.

Tables 6 and 7 provide a list of the strain tensors in the observation system according to the model of Cortés-Pérez [29] and the $|SR|$ for each expected MV (only the first three cases satisfying

these conditions were analyzed). In these tables, the positions of the three MVs with higher $|SR|$ reflect the order of the SF from maximum to minimum. The MVs with a high $|SR|$ are coincident for the majority of all studied grains. However, several cases or inconsistencies were observed in the comparison of Tables 2–5 with Tables 6 and 7, as described below.

- (a) In some cases, the ϵ_{x0} values are negative; however, this situation is not possible because deformation against the movement is implicated. In other words, these values indicate negative SFs. Therefore, these values for the SR criterion should be discarded in this analysis. For example, MVs 11 and 3 in grain 42 present the case mentioned above; the maximum $|SR|$ in grain 42 is present in MV 2. For this reason, the MV with negative ϵ_{x0} will be discarded in the next subsections. Therefore, the next $|SR|$ with a positive value of ϵ_{x0} will be considered the maximum $|SR|$. Despite the aforementioned information, possible negative values of ϵ_{x0} in MVs were found that coincided with the real MV formed. For example, the MV 23 in grain 63 is coincident with real MV 63-I.
- (b) If an MV has a higher $|SR|$, it may coincide instead of the MV with the higher SF (this result occurs for grains 42, 94, and 96 in our sample).

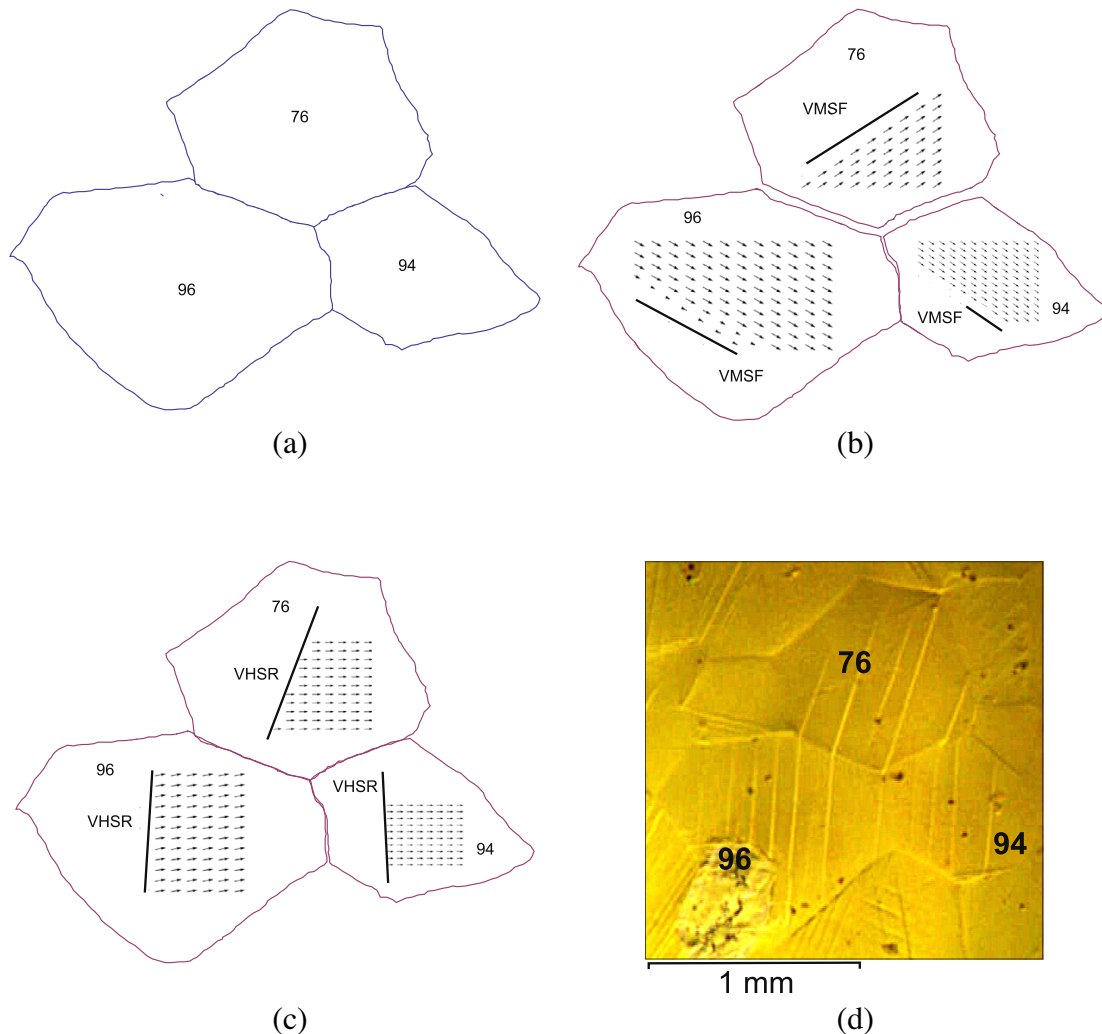


Fig. 6. Comparison between the two grain boundaries under the SIMT for region 2. (a) Original configuration. (b) Distortion using the MV with maximum SF (VMSF), and (c) distortion using the MV formed with higher SR ($\epsilon_{x0}/\epsilon_{y0}$) (VHSR). (d) Real MVs formed in each grain.

Table 6
Strain tensor analysis for our grains according to the |SR| criterion using the model of Cortés–Pérez [29].

Region	Grain	Expected MVs	Strain tensor $\begin{pmatrix} \varepsilon_{x0} & \gamma_{xy0} \\ \gamma_{xy0} & \varepsilon_{y0} \end{pmatrix}$	Highest values SR	Coincident MV with calculated MV	Position in SF	
1	42	11*	$\begin{pmatrix} 0.08117 & 0.0174 \\ 0.0174 & -0.00165 \end{pmatrix}$	49.19	None	20	
		3*	$\begin{pmatrix} -0.06085 & 0.01592 \\ 0.01592 & -0.00166 \end{pmatrix}$	36.66	42-II	17	
		2	$\begin{pmatrix} 0.08836 & 0.01694 \\ 0.01694 & -0.00266 \end{pmatrix}$	33.22	42-I	3	
	43	11	$\begin{pmatrix} 0.0844 & 0.02039 \\ 0.02039 & 0.00485 \end{pmatrix}$	17.40	43-I	1	
		3	$\begin{pmatrix} 0.06628 & 0.01601 \\ 0.01601 & 0.0039 \end{pmatrix}$	16.99	43-I	3	
		12*	$\begin{pmatrix} -0.06199 & -0.02753 \\ -0.02753 & -0.00965 \end{pmatrix}$	6.42	43-I	22	
	63	23*	$\begin{pmatrix} -0.1106 & -0.00142 \\ -0.00142 & 0.01677 \end{pmatrix}$	6.60	63-I	22	
		18*	$\begin{pmatrix} 0.1014 & 0.01013 \\ 0.01013 & 0.0176 \end{pmatrix}$	5.76	63-II	18	
		17	$\begin{pmatrix} 0.09701 & 0.0208 \\ 0.0208 & -0.03213 \end{pmatrix}$	3.02	63-II	6	
		76	22	$\begin{pmatrix} 0.05533 & -0.01444 \\ -0.01443 & -0.0001 \end{pmatrix}$	553.3	None	5
	2	76	17	$\begin{pmatrix} 0.077 & -0.01369 \\ -0.01369 & -0.00087 \end{pmatrix}$	88.51	76-I	3
			20*	$\begin{pmatrix} -0.044 & 0.05097 \\ 0.05097 & -0.00151 \end{pmatrix}$	29.14	None	17
94			15	$\begin{pmatrix} 0.08542 & 0.00104 \\ 0.00104 & 0 \end{pmatrix}$	∞	94-I	3
94		6	$\begin{pmatrix} 0.06532 & 0.00033 \\ 0.00033 & 0 \end{pmatrix}$	∞	94-I	5	
		5*	$\begin{pmatrix} -0.07623 & -0.03618 \\ -0.03618 & 0.0004 \end{pmatrix}$	190.58	94-I	20	
96		22*	$\begin{pmatrix} 0.08413 & -0.02460 \\ -0.02460 & 0.0005 \end{pmatrix}$	168.2	None	23	
		18	$\begin{pmatrix} 0.09087 & 0.00532845 \\ 0.00533 & -0.00081 \end{pmatrix}$	112.19	96-I	2	
		23	$\begin{pmatrix} 0.073 & 0.00071 \\ 0.00071 & -0.0018 \end{pmatrix}$	40.56	None	4	

* ε_{x0} negative.

Table 7
Strain tensor analysis for the grains reported by Kaouache et al. [27] using the model of Cortés–Pérez [29].

Sample	Grain	Expected MVs	Strain tensor $\begin{pmatrix} \varepsilon_{x0} & \gamma_{xy0} \\ \gamma_{xy0} & \varepsilon_{y0} \end{pmatrix}$	Maximum values SR	Coincident MV with calculated MV	Position in SF
P1	A1	4	$\begin{pmatrix} 0.09755 & -0.04089 \\ -0.04164 & 0.01391 \end{pmatrix}$	7.01	A1-I	1
		10	$\begin{pmatrix} 0.08854 & -0.04095 \\ -0.04164 & 0.01595 \end{pmatrix}$	5.55	None	2
		9*	$\begin{pmatrix} -0.07021 & 0.06329 \\ 0.06452 & -0.02603 \end{pmatrix}$	2.70	None	22
	B1	21	$\begin{pmatrix} 0.07463 & -0.04801 \\ -0.04858 & 0.00060 \end{pmatrix}$	124.38	B1-III	3
		19*	$\begin{pmatrix} -0.07887 & 0.01508 \\ 0.01528 & -0.00072 \end{pmatrix}$	109.54	None	19
		24*	$\begin{pmatrix} -0.05748 & 0.01657 \\ 0.01684 & -0.00153 \end{pmatrix}$	37.57	None	17
	C1	20*	$\begin{pmatrix} -0.10456 & -0.03355 \\ -0.0344 & 0.00139 \end{pmatrix}$	75.22	C1-II	23
		21*	$\begin{pmatrix} -0.09305 & -0.03988 \\ -0.04062 & -0.00328 \end{pmatrix}$	28.37	C1-III	18
		19	$\begin{pmatrix} 0.07585 & 0.06567 \\ 0.06703 & 0.00465 \end{pmatrix}$	16.31	C1-II	8
		P2	A2	4*	$\begin{pmatrix} -0.04876 & -0.0531 \\ -0.05455 & 0.00011 \end{pmatrix}$	443.27
5*	$\begin{pmatrix} -0.03405 & 0.08884 \\ 0.09024 & -0.00024 \end{pmatrix}$			141.86	A2-II	16
23	$\begin{pmatrix} 0.08958 & -0.05145 \\ -0.05174 & 0.00237 \end{pmatrix}$		37.80	A2-II	2	

* ε_{x0} negative.

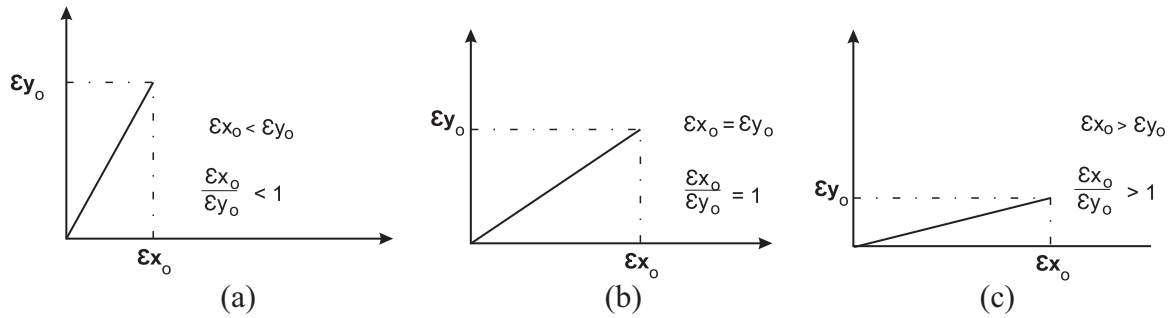


Fig. 7. Cases presented for |SR|. (a) Deformation near TD. (b) Deformation of the middle of TD and RD. (c) Deformation near RD.

Table 8 Selected MVs using the |SR|–SF criterion for grain 42.

Grain 42					
SR	MV	Status	SF	MV	Status
49.09	11	C	0.47	19	D
36.62	3	A, C	0.42	24	D
33.17	2	A, B	0.38	2	A, B
30.74	12	B	0.30	17	D
5.69	9	A, C	0.30	4	A, B
5.43	4	A, B	0.30	12	B
5.20	10	A, B	0.26	22	D
3.95	1	C	0.22	10	A, B
0.98	19	D	0.17	16	D
0.96	24	D	0.15	7	D
0.94	23	D	0.02	13	D
0.86	18	D	0.002	14	D
0.83	20	D	–0.009	5	C
0.83	21	D	–0.02	8	C
0.62	17	D	–0.08	15	C
0.57	22	D	–0.08	6	C
0.36	16	D	–0.26	3	C
0.34	7	D	–0.31	1	C
0.18	15	D	–0.33	18	C
0.17	6	D	–0.35	11	C
0.04	13	D	–0.38	9	A, C
0.04	8	D	–0.38	20	C
0.02	5	D	–0.39	23	C
0.003	14	D	–0.41	21	C

- (A) Coincident MV according to Table 4.
- (B) MV with a high probability of appearing.
- (C) Discarded MV with negative SF.
- (D) Discarded MV with |SR| < 1.

Table 9 Vs predicted using the |SR|–SF criterion for grain 42.

Grain 42								
SRp*	SR	MV	Status	SFp**	SF	MV	Status	Order value (Ov)
3rd	33.17	2	A, B	3rd	0.38	2	A, B	10
4th	30.74	12	B	4th	–	–	–	9
5th	–	–	–	5th	0.30	4	A, B	8
6th	5.43	4	A, B	6th	0.30	12	A, B	7
7th	5.20	10	A, B	7th	–	–	–	6
8th	–	–	–	8th	0.22	10	A, B	5

- (A) Coincident MV according to Table 2.
- (B) MV with a high probability of appearing.
- * Strain ratio position.
- ** Schmid factor position.

- (c) Despite there being an MV with the maximum |SR|, this does not imply that this MV will appear. For example, grain 76 indicated that MV 22 with a high |SR| did not coincide with the MV plotted.
- (d) For each real MV formed in a grain, two or more MVs that are coincident with this MV may exist. For example, in grain 43, MVs 11 and 3 presented a high |SR| and the same line in the

Table 10 Possible order of growth of MVs predicted according to the BC between |SR| and SF for grain 42.

Grain 42	
MV	BC value
2	10
12	7
4	6
10	5

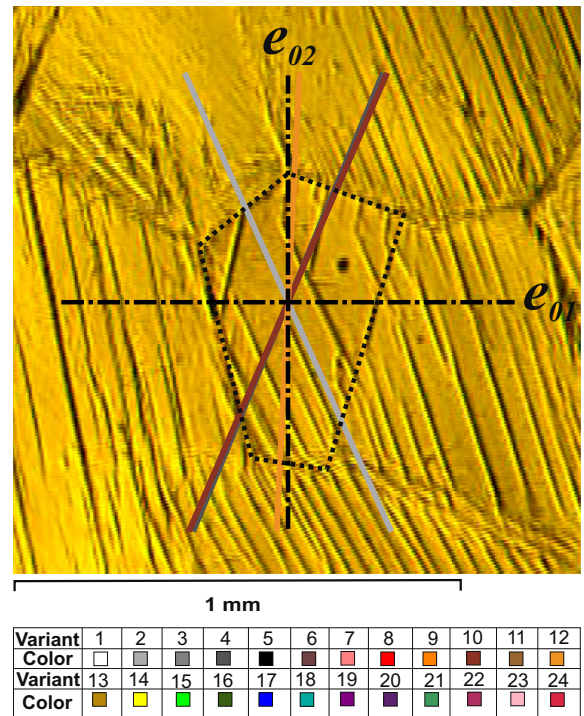


Fig. 8. Predicted MVs for grain 42 of region 1.

- observation system; however, only one of these MVs was formed (Fig. 4a). It is difficult to select an MV when the MVs present very similar values.
- (e) For grains with two or three real MVs formed, it is not possible to know which MVs coincide with the principal or which will grow first, e.g., grains 42, 63, B1, C1 and A2.
- (f) Some grains present MVs with very similar value of SF; however, only one is coincident, e.g., grain 63 and its MVs 19 and 2.

Table 11
Selected MVs using the |SR|–SF criterion for grain 96.

Grain 96					
SR	MV	Status	SF	MV	Status
168	22	C	0.41	13	D
112.73	18	A, B	0.39	18	A, B
40.6	23	B	0.33	8	D
12.74	17	A, C	0.31	23	B
7.31	24	C	0.25	15	D
5.06	19	C	0.25	20	B
1.86	20	B	0.19	6	D
1.52	21	B	0.19	21	B
0.97	13	D	0.12	2	D
0.96	8	D	0.10	3	D
0.87	7	D	0.08	12	D
0.87	14	D	0.05	11	D
0.86	5	D	−0.03	4	C
0.80	16	D	−0.05	1	C
0.59	15	D	−0.05	10	C
0.52	6	D	−0.07	9	C
0.29	3	D	−0.23	19	C
0.27	2	D	−0.24	16	C
0.20	12	D	−0.30	17	A, C
0.15	11	D	−0.32	14	C
0.14	9	D	−0.32	24	C
0.13	10	D	−0.32	7	C
0.11	1	D	−0.36	22	C
0.08	4	D	−0.37	5	C

- (A) Coincident MV according to Table 2.
- (B) MV with a high probability of appearing.
- (C) Discarded MV with negative SF.
- (D) Discarded MV with |SR| < 1.

Table 12
Selected MVs using the |SR|–SF criterion for grain A1 of Kaouache et al. [27].

Grain A1					
SR	MV	Status	SF	MV	Status
7.01	4	A, B	0.42	4	A, B
5.55	10	B	0.38	10	B
2.70	9	C	0.26	6	B
2.11	23	C	0.24	24	B
2.01	11	A, C	0.23	15	B
2.01	3	A, C	0.21	2	D
1.74	1	C	0.18	12	A, D
1.42	18	C	0.17	22	D
1.23	6	B	0.14	19	B
1.17	15	B	0.07	17	D
1.05	19	B	0.05	8	D
1.04	24	B	0.03	13	D
0.98	20	D	−0.06	7	C
0.96	21	D	−0.10	21	C
0.79	22	D	−0.10	16	C
0.78	2	D	−0.15	5	C
0.69	17	D	−0.16	23	C
0.63	12	A, D	−0.16	14	C
0.53	5	D	−0.21	20	C
0.49	14	D	−0.25	1	C
0.32	16	D	−0.25	18	C
0.19	7	D	−0.30	9	C
0.12	8	D	−0.32	3	A, C
0.08	13	D	−0.33	11	A, C

- (A) Coincident MV according to Table 4.
- (B) MV with a high probability of appearing.
- (C) Discarded MV with negative SF.
- (D) Discarded MV with |SR| < 1.

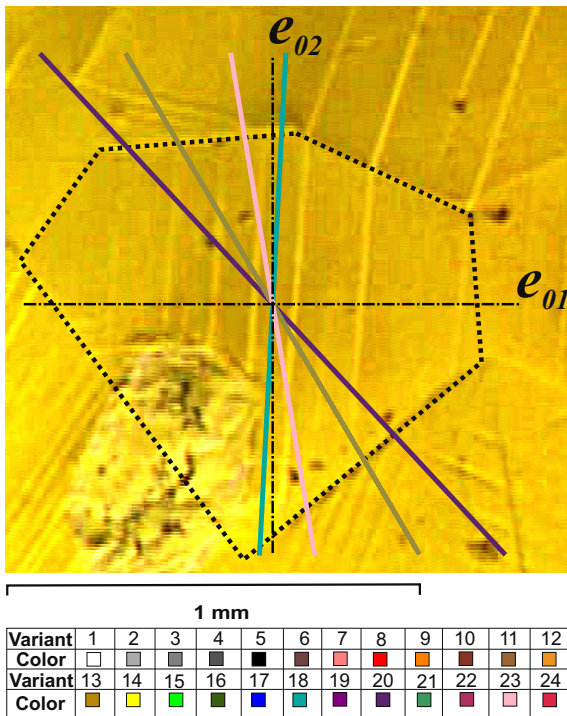


Fig. 9. Predicted MVs for grain 96 of region 2.

(g) Values of |SR| with infinite value are always coincident, e.g., MVs 15 and 6 of grain 94.

For both criteria, the SF and |SR| clearly presented some inconsistencies with the real MVs formed. Therefore, it was not possible to predict which MV would appear.

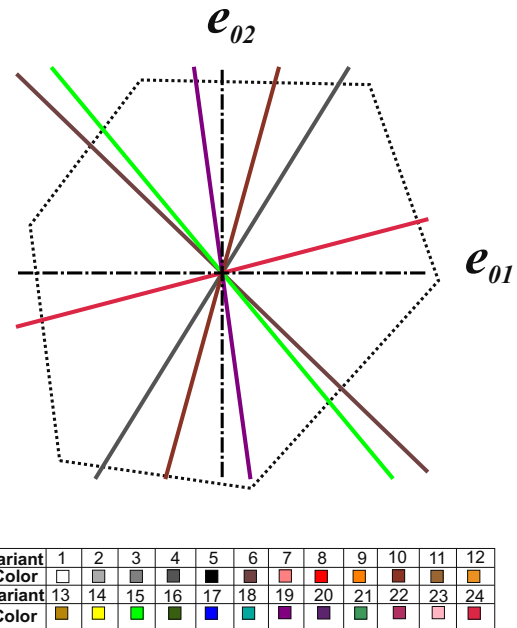


Fig. 10. Predicted MVs for grain A1 of sample P1 from Kaouache et al. [27].

For these reasons, a new criterion involving a combination of both the SF and |SR| (or SR and $-\epsilon_{x0}$) criteria was proposed in this research. This criterion involves the following considerations:

- (1) MVs with negative SF are discarded.
- (2) MVs with |SR| < 1 are discarded because this situation implies that ϵ_{x0} is less than ϵ_{y0} ; furthermore, this state of strain is not favored by the applied load direction (RD), as shown in Fig. 7.

Table 13

Summary of the results applying the BC for grains of our sample and those of Kaouache et al. [27].

Grain	Expected MVs with BC	Number of formed MVs per grain	Coincident MVs
42	2, 12, 4, 10	I	2
		II	4, 10
43	11, 3	I	11, 3
63	17, 24, 19, 22, 12, 2, 4, 10	I	24
		II	19, 10
		III	17, 24
76	22, 17, 19, 24, 2, 12	I	17
94	15, 6, 13, 8	I	15, 6
96	18, 23, 20, 21	I	18
A1	4, 10, 6, 15, 19, 24	I	4
B1	21, 20, 23, 18, 6, 15	I	6
		II	15
		III	21
C1	24, 19, 22, 17, 4, 2, 10, 12	I	24, 17, 10
		II	19
		III	22
A2	23, 11, 18, 3, 15, 20	I	18
		II	23
		III	3

(3) A balance criterion (BC) based on the following equations should be used with the remaining MVs:

$$\text{If } SF_p \leq SR_p \quad BC = (SF_p - SR_p) + O_v \quad (16a)$$

$$\text{and if } SR_p \leq SF_p \quad BC = (SR_p - SF_p) + O_v \quad (16b)$$

where SF_p and SR_p are the positions of SF and SR respectively. O_v is an integer number with a maximum value of 10 that prioritizes the

positions of SF and/or SR that were not discarded under considerations 1 and 2.

Table 8 presents the complete list of the $|SR|$ and SF values for grain 42. Notice that $|SR|$ does not depend on the shear amplitude. In this table, our proposed criteria were applied until consideration 2, and the coincident MVs (A) and the discarded MVs (C, D) were labeled with letters. The coincident MVs are presented in Table 2. The predicted MVs were then 2, 12, 4, and 10, as shown in Table 9.

Table 9 shows the MVs with status A and B (or only B) according to Table 8. In both cases, the same MVs are obtained for $|SR|$ and SF ; however, their order of appearance differs. For this reason, the third consideration must be included (this last consideration is not necessary if the SR and $-\epsilon_{x0}$ are considered). We took into account both criteria ($|SR|$ and SF); until now, these criteria have had the same importance, and their influence has been weakened when their values are small. MV 2 has the same position (3rd) for the $|SR|$ and SF ; therefore, this MV is the first MV with the greatest probability of appearing. However, the aforementioned condition is not always present; for example, MV 12 occupies the 4th position according to the $|SR|$ value but the 6th position with respect to SF . In this case, it is difficult to predict the order of MV formation. For this reason, a BC was introduced. This balancing criterion is used to propose an ordering of MVs by probability of appearance based on an assigned order value (O_v), which will depend on the largest values of the $|SR|$ position (SR_p) and SF position (SF_p). This BC is summarized in Eqs. (16a) and (16b). Note that if $SF_p = SR_p$, both equations can be used interchangeably. For example, the ideal case occurs when an MV has the same position in $|SR|$ and SF and their values are maximal. In MV 2, we obtained a BC value of 10 using Eqs. (16a) or (16b), $BC = (|3 - 3| + 10 = 10)$; this value indicates the best balance and corresponds to MV 2. MV 12 is in the fourth position according to the $|SR|$ but the sixth position according to its SF ; this condition has a BC value of 7 (in this case, Eq. 16b

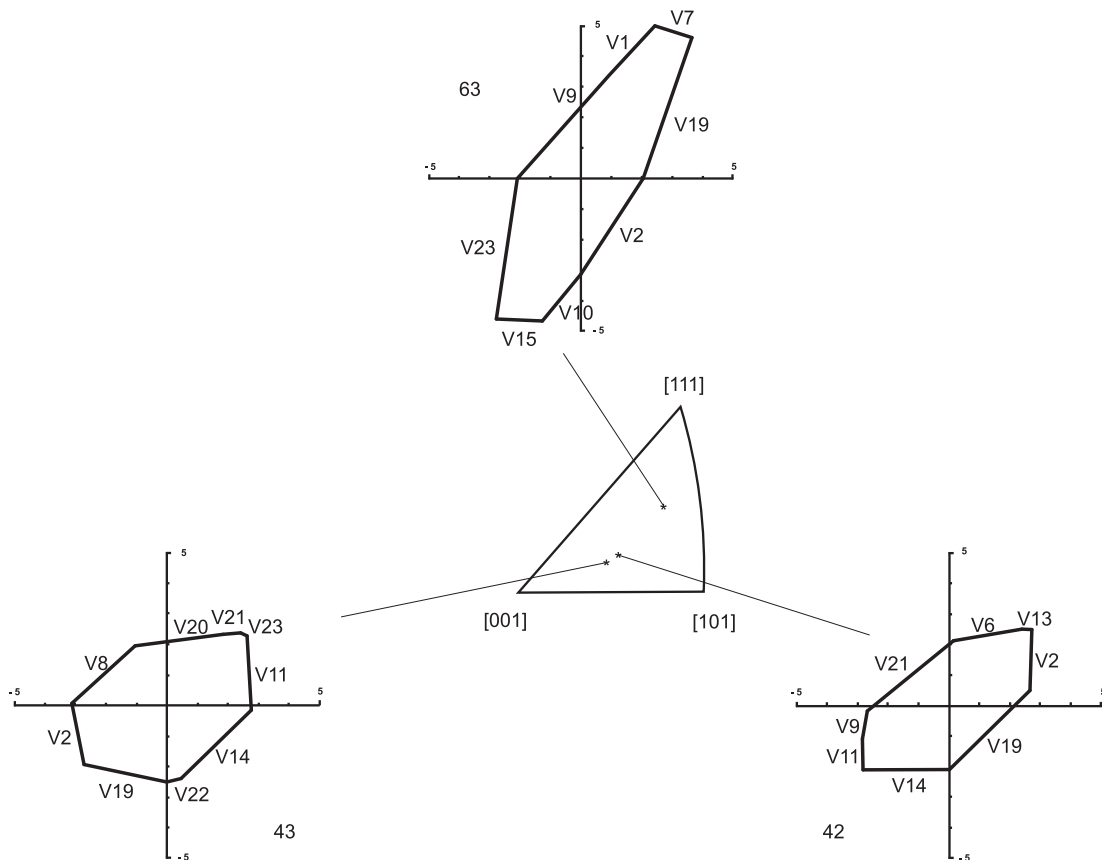


Fig. 11. STDs for region 1 involving grains 42, 43, and 63; these diagrams present the predicted MVs as a function of the crystal orientation and state of stress.

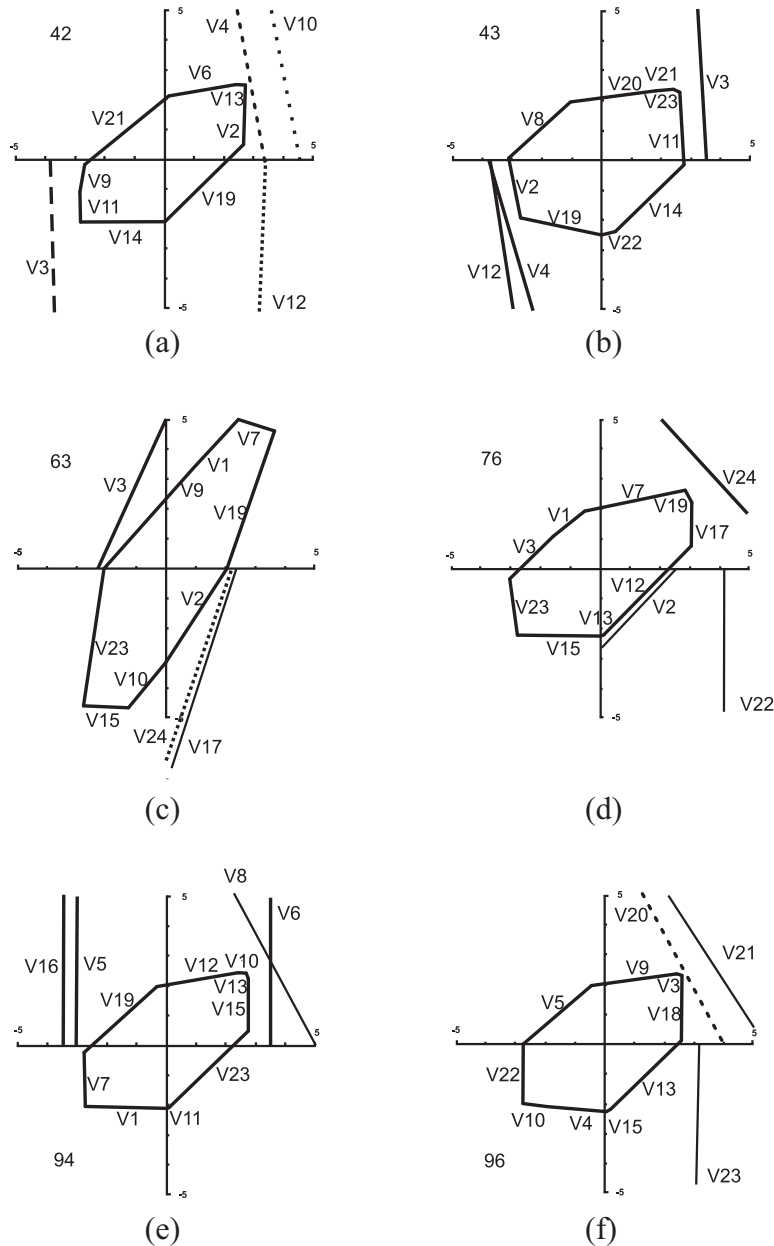


Fig. 12. Calculated STDs for the grains 42, 43, 63, 76, 94, and 96 in the Cu–Al–Be system.

was used because $SR_p \leq SF_p$ ($[4 - 6] + 9 = 7$). Following the *BC* and their conditions, the order of growth was determined for *MVs* 4, 10 and 12 in grain 42, as shown in Table 10. The predicted *MVs* are shown in Fig. 8. Similarly, the $|SR|$ and SF values for grain 96 are presented in Table 11.

When the methodology used for grain 42 was applied to grain 96, the predicted *MVs* were 18, 23, 20, and 21. *MV* 18 was the most balanced because this *MV* had high values of both SF and $|SR|$; this *MV* was the principal *MV* predicted, and it had a *BC* value of 10. The next *MVs*, 23 and 20, did not have a similar equilibrium relation and had *BC* values of 7 and 3, respectively. Finally, *MV* 21 had a similar position but less balance than the previous *MVs* ($[8 - 8] + 2 = 2$). The predicted *MVs* are shown in Fig. 9.

Finally, the application of our criteria for grain A1 is presented in Table 12.

In this case, more *MVs* satisfied the proposed criteria, with the following order of possible growth: 4, 10, 6, 15, 19, and 24. This order is based on the *BC* values. *MVs* 4 and 10 exhibited higher *BC* values of 10 and 9, respectively. The *BC* of the remaining *MVs* was small. For example, the next *MVs*, 6 and 15, had *BC* values of 2 and 1, and the last *MVs*, 19 and 24, actually had zero or negative values under our criterion. The 6 predicted *MVs* for this case are presented in Fig. 10.

Table 13 presents the predicted *MVs* for all the grains studied here.

All maximum values for *BC* are shown in the second column, whereas the *MVs* that are coincident with the *BC* according to the *MVs* listed in Tables 2 and 4 are shown in the last columns. For example, the expected *MVs* in grain 42 are 2, 12, 4, and 10; however, only *MVs* 2, 4 and 10 have lines that are coincident with

the MVs formed. Therefore, these MVs are predicted in grain 42. Similarly, the MVs predicted in the other grains are selected using the methodology described above. Close agreement is observed between our proposed criteria and the actual MVs formed in all the grains studied because the expected MV always appeared.

The proposed BC is in agreement with the experimental results but exhibits some inconsistencies. (a) For example, in grain 42, MVs 4 and 10 are coincident with a real formed MV. The cases for grains 43, 94, 96, and C1 are similar. (b) MVs were predicted but not observed at that particular state of stress when the metallographic images were captured. For example, in the case of grain A1, MV 10 was formed according to Kaouache et al. [28]; however, MV 10 was inhibited under the high-stress condition.

To improve the proposed criterion, we included the in-plane STDs as a discrimination tool, which allows us to predict the stress-induced MV in a polycrystalline SMA when combined with our BC developed above. Thus, we calculated the transformation diagrams for all the studied grains using the procedure presented by Buchheit et al. and Comstock et al. [14,15]. Fig. 11 presents the STDs for region 1 and their location in the inverse pole diagram. The STD diagrams are valid for an in-plane state of stress in single crystals.

The STD has four quadrants (according to a Cartesian system) with different states of stress: the first quadrant corresponds to tension–tension ($T-T$), the second quadrant to compression–tension ($C-T$), the third quadrant to compression–compression ($C-C$) and the fourth quadrant to tension–compression ($T-C$). For example, MVs 1, 7, and 19 will appear in grain 63 if the state of stress is $T-T$, as shown in Fig. 11. However, these diagrams should be modified for polycrystals because of the GI effect. Fig. 12 presents the transformation diagram for the grains of our sample, and Fig. 13 presents the transformation diagrams for the grains

studied by Kaouache et al. [27]. Figs. 12 and 13 consider the coincident MVs listed in Tables 2 and 4, respectively, whereas the MVs expected with the BC are shown in Table 13.

In all grains, the MVs in the second and third quadrant are discarded because their states of stress differ from simple tension ($C-C$ and $C-T$). Fig. 12a presents the STD for grain 42. In this case, the MVs discarded in quadrants two and three are 9, 11, 14, and 21. The case of MV 3 is shown because this MV appeared in Table 2. In contrast, the MVs located in quadrants one and four have a high probability of appearing. In fact, if the grain boundary does not exist, the uniquely formed MV in tension will be MV 19; this MV corresponds to the maximum SF. However, this MV is discarded by the BC; therefore, according to the proposed criterion, MV 2 is expected and is in agreement with the STD. The next predicted MVs with the BC criterion are MVs 4, 12 and 10; the transformation diagram clearly illustrates that MV 4 has the highest probability of appearing because less energy is needed for its formation. In the case of MVs 6 and 13, the state of stress is high in the TD, and these MVs are discarded as well. Finally, MVs 2 and 4 are the predicted MVs for the combination of the $|SR|$ -SF criterion and the transformation diagram. In the case of grain A1, the discarded MVs in quadrants two and three are 8, 18, 11, 14, 16, 7 and 3. The expected MVs for BC are 4, 10, 6, 15, 19 and 4; the MV predicted in this case is clearly MV 4. This MV has the maximum SF and is uniquely formed according to Kaouache et al. [27]. The mechanism is shown in BC; this MV has the highest BC values, and the other MVs are less likely to appear. However, MV 10 has a good BC relation; in fact, this MV was formed at low deformation, in agreement with Kaouache [28].

Finally, this methodology was applied to all the studied grains, and the results were consistent with the proposed criterion. The final criterion is the combination of BC and STD, and the SIMT need

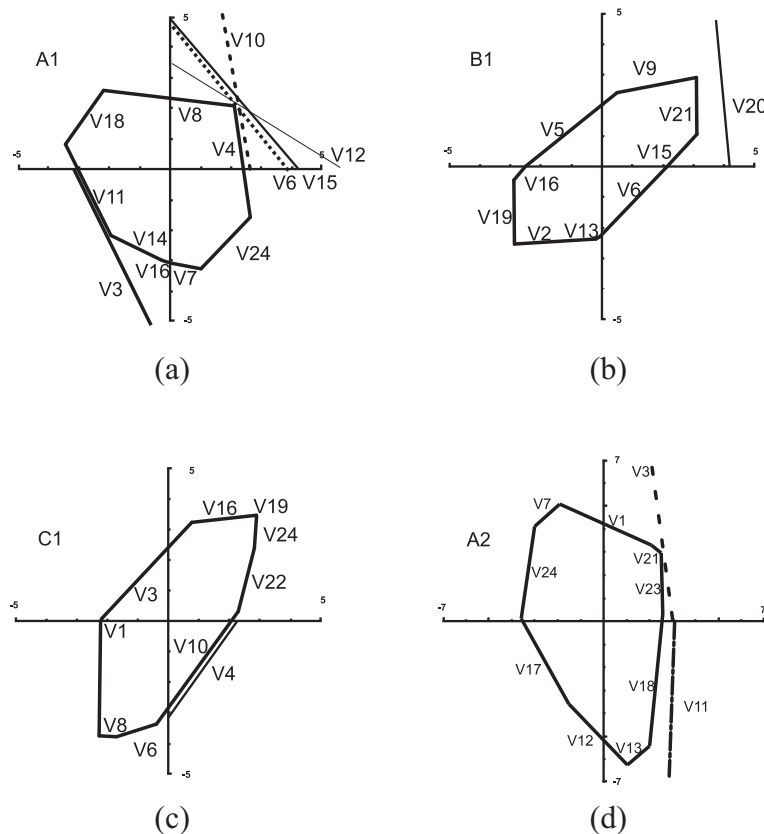


Fig. 13. Calculated STDs for the grains A1, B1, C1, and A2 previously studied by Kaouache et al. [27].

Table 14
Summary of the results of the *MVs* predicted with the *BC-STD* criterion.

Grain	Number of <i>MVs</i> formed	Variants predicted with <i>BC-STD</i>
42	I	2
	II	4
43	I	11
	II	19
63	I	24
	III	17
76	I	17
94	I	15
96	I	18
A1	I	4
	II	6
B1	I	15
	II	21
	III	10
C1	I	19
	II	22
	III	18
A2	I	23
	II	3
	III	

not be observed in situ. Importantly, using our methodology and the Cortés–Pérez model [29], the mechanical behavior of a polycrystalline Cu–Al–Be *SMA* may be estimated if the crystalline orientation is known. Furthermore, our methodology can be applied to study the yield in conventional polycrystalline materials because the mechanism of martensitic transformation is similar to the slip plane, which is well known and relevant to explaining yield. A summary of the predictions for all the studied grains is provided in Table 14.

4. Conclusions

According to the literature, the nature of the *SIMT* can be studied using the *SF* criterion; however, in our research, some inconsistencies have been observed for specific grains. Our results demonstrate that grain boundary interaction modifies the state of stress that favors or inhibits the growth of specific *MVs*; this modification explains why the third or second *MV* with a high *SF* value grows instead of the *MV* with maximum *SF*. To better understand the nature of the *SIMT*, the *SR* was used. However, the use of the *SF* and $|SR|$ criteria to predict the formation of *MVs* resulted in several inconsistencies. Furthermore, the *BC-STD* criterion, which predicts which *MVs* have a high probability of appearing and the possible order of formation of *MVs*, was developed. To apply our criterion, the following parameters must be considered: the crystallographic orientation, transformation system, critical temperatures of transformation, grain geometry, magnitude of shear, test temperature, and magnitude of the applied normal stress during the uniaxial tensile test. Although the *BC-STD* criterion does not consider the interaction between martensitic–martensitic variants or changes in the stress distribution associated with evolution/reorientation of *MVs*, the *BC-STD* criterion shows good agreement with the experiment results. In addition, it demonstrates the strong influence of crystallographic orientation in the *MVs* formed during the *SIMT*.

Acknowledgments

The authors wish to thank the Coordinación de estudios de posgrado (CEP)–UNAM, PAPIIT project number TI 02414 and Instituto de Tecnología de Materiales–UPV for financial support. The authors are grateful to the Electron Microscopy Service of the UPV and

especially to Manuel Josep Planes Insausti and José Luis Moya López. The authors are grateful to Martín Estrada Arcos, Alberto Higuera García, and Antonio González Montañón for their technical support.

References

- [1] K.N. Melton, General applications of *SMA*'s and smart materials, in: K. Otsuka, C.M. Wayman (Eds.), *Shape Memory Materials*, Cambridge University Press, Cambridge, 1998, pp. 220–239.
- [2] P.K. Kumar, D.C. Lagoudas, Introduction to shape memory alloys, in: D.C. Lagoudas (Ed.), *Shape Memory Alloys. Modeling and Engineering Applications*, Springer, New York, 2008, pp. 1–43.
- [3] H. Tobushi, K. Date, K. Miyamoto, Characteristics and development of shape-memory alloys heat engine, *J. Solid. Mech. Mater. Eng.* 4 (2010) 1094–1102.
- [4] K. Kaneko, K. Enomoto, Development of reciprocating heat engine using shape memory alloys, *J. Environ. Eng.* 6 (2011) 131–139.
- [5] J.J. Zhu, N.G. Liang, K.M. Liew, W.M. Huang, Energy conversion in shape memory alloy heat engine Part I: theory, *J. Intell. Mater. Syst. Struct.* 12 (2001) 127–132.
- [6] J.J. Zhu, N.G. Liang, W.M. Huang, K.M. Liew, Energy conversion in shape memory alloy heat engine Part II: simulation, *J. Intell. Mater. Syst. Struct.* 12 (2001) 133–140.
- [7] K. Otsuka, C.M. Wayman, Mechanism of shape memory effect and superelasticity, in: K. Otsuka, C.M. Wayman (Eds.), *Shape Memory Materials*, Cambridge University Press, Cambridge, 1998, pp. 27–48.
- [8] V. Novák, P. Šittner, N. Zárubová, Anisotropy of transformation characteristics of Cu–base shape memory alloys, *Mater. Sci. Eng. A* 234–236 (1997) 414–417.
- [9] V. Novák, P. Šittner, D. Vokoun, N. Zárubová, On the anisotropy of martensitic transformations in Cu–based alloys, *Mater. Sci. Eng. A* 273–275 (1999) 280–285.
- [10] K. Otsuka, X. Ren, Physical metallurgy of Ti–Ni–based shape memory alloys, *Prog. Mater. Sci.* 50 (2005) 511–678.
- [11] K. Taillard, S. Arbab Chirani, S. Calloch, C. LExcellent, Equivalent transformation strain and its relation with martensite volume fraction for isotropic and anisotropic shape memory alloys, *Mech. Mater.* 40 (2008) 151–170.
- [12] E. Patóor, D.C. Lagoudas, P.B. Entchev, L.C. Brinson, X. Gao, Shape memory alloys, Part I: general properties and modeling of single crystals, *Mech. Mater.* 38 (2006) 391–429.
- [13] X. Gao, M. Huang, L.C. Brinson, A multivariant micromechanical model for *SMA*s Part 1. Crystallographic issues for single crystal model, *Int. J. Plast.* 16 (2000) 1345–1369.
- [14] T.E. Buchheit, J.A. Wert, Modeling the effects of stress state and crystal orientation on the stress-induced transformation of Ni–Ti single crystals, *Metall. Mater. Trans. A* 25 (1994) 2383–2389.
- [15] R.J. Comstock, T.E. Buchheit, M. Somerday, J.A. Wert, Modeling the transformation stress of constrained shape memory alloy single crystals, *Acta Mater.* 44 (1996) 3505–3514.
- [16] B.C. Goo, C. LExcellent, Micromechanics-based modeling of two-way memory effect of a single crystalline shape-memory alloy, *Acta Mater.* 45 (1997) 727–737.
- [17] D.C. Lagoudas, P.B. Entchev, P. Popov, E. Patóor, L.C. Brinson, X. Gao, Shape memory alloys, Part II: modeling of polycrystals, *Mech. Mater.* 38 (2006) 430–462.
- [18] Z.K. Lu, G.J. Weng, A self-consistent model for the stress-strain behavior of shape-memory alloy polycrystals, *Acta Mater.* 46 (1998) 5423–5433.
- [19] M. Panico, L.C. Brinson, A three-dimensional phenomenological model for martensite reorientation in shape memory alloys, *J. Mech. Phys. Solids.* 55 (2007) 2491–2511.
- [20] P. Šittner, V. Novák, Experiment feedbacks in micromechanics modeling of thermomechanical behaviors of *SMA* polycrystals, *Scr. Mater.* 51 (2004) 321–326.
- [21] S. Montecinos, A. Cuniberti, A. Sepúlveda, Grain size and pseudoelastic behaviour of a Cu–Al–Be alloy, *Mater. Charact.* 59 (2008) 117–123.
- [22] S. Berveiller, B. Malard, J. Wright, E. Patóor, G. Geandier, In situ synchrotron analysis of lattice rotations in individual grains during stress-induced martensitic transformations in a polycrystalline CuAlBe shape memory alloy, *Acta Mater.* 59 (2011) 3636–3645.
- [23] N. Siredey, E. Patóor, M. Berveiller, A. Eberhardt, Constitutive equations for polycrystalline thermoelastic shape memory alloys. Part I. Intragranular interactions and behavior of the grain, *Int. J. Solids Struct.* 36 (1999) 4289–4315.
- [24] F.M. Sánchez-Arévalo, G. Pulos, Use of digital image correlation to determine the mechanical behavior of materials, *Mater. Charact.* 59 (2008) 1572–1579.
- [25] R.J. Martínez-Fuentes, F.M. Sánchez-Arévalo, F.N. García-Castillo, G.A. Lara-Rodríguez, J. Cortés-Pérez, A. Reyes-Solis, Micromechanical behavior of CuAlBe shape memory alloy undergoing 3-point bending analyzed by digital image correlation, in: Francisco Manuel Braz Fernandez (Ed.), *Shape Memory Alloys – Processing, Characterization and Applications*, InTech, Rijeka, 2013, pp. 197–212.

- [26] N. Bourgeois, F. Meraghni, T.B. Zineb, Measurement of local strain heterogeneities in superelastic shape memory alloys by digital image correlation, *Phys. Proc.* 10 (2010) 4–10.
- [27] B. Kaouache, K. Inal, S. Berveiller, A. Eberhardt, E. Patoor, Martensitic transformation criteria in Cu–Al–Be shape memory alloy—In situ analysis, *Mater. Sci. Eng. A* 438–440 (2006) 773–778.
- [28] B. Kaouache (Doctorate thesis), ENSAM, CER de Metz, 2006.
- [29] J. Cortés (Ph.D. thesis), Facultad de Ingeniería UNAM, Distrito Federal, 2007.
- [30] S. Belkahla (Ph.D. thesis), INSA Lyon, 1990.
- [31] H. Flores (Ph.D. thesis), Inst. Nat. Sc. Appl., Lyon, 1993.
- [32] A. Tidu, A. Eberhardt, B. Bolle, F. Moreau, J.-J. Heizmann, Orthorhombic lattice deformation of CuAlBe shape-memory single crystals under cyclic strain, *J. Appl. Cryst.* 34 (2001) 722–729.
- [33] A. Hautcoeur, A. Eberhard, E. Patoor, Berveiller, Thermomechanical behavior of monocrystalline Cu–Al–Be shape memory alloys and determination of the metastable phase diagram, *J. Phys.* 05 (1995) 459–464.
- [34] S. Kajiwara, Theoretical analysis of the crystallography of the martensitic transformation of BBC to 9R close-packed structure, *Trans. Jpn. Inst. Met.* 17 (1976) 435–446.
- [35] J. Cortés-Pérez, J.G. González, J. Carrera, H. Flores. Mathematical analysis of experimental results in polycrystalline shape memory samples subject to a simple uniaxial tension test, in: P. Šittner, L. Heller and V. Paidar, Paidar (Eds.), ESOMAT 2009. The 8th European Symposium on Martensitic Transformations, Sciences, 2009, pp. 1–6.